The Astronomical Journal, 138:770–779, 2009 September doi:10.1088/0004-6256/138/3/770

AN *HST*/WFPC SURVEY OF BRIGHT YOUNG CLUSTERS IN M31. II. PHOTOMETRY OF LESS LUMINOUS CLUSTERS IN THE FIELDS

P. W. Hodge[1], O. K. Krienke[2], M. Bellazzini[3], S. Perina[3], P. Barmby[4], J. G. Cohen[5], T. H. Puzia[6], and J. Strader[7]
[1] Department of Astronomy, University of Washington, Seattle, WA 98195-1580, USA
[2] Seattle Pacific University, Seattle, WA 98119, USA
[3] INAF-Osservatorio di Bologna, via Ranzani 1, 40127 Bologna, Italy
[4] Department of Physics and Astronomy, University of Western Ontario, London, ON N6A 3K7, Canada
[5] Palomar Observatory, Mail Stop 105–24, California Institute of Technology, Pasadena, CA 91125, USA
[6] Herzberg Institute of Astrophysics, 5071 West Saanich Rd., Victoria, BC, V9E 2E7, Canada
[7] Harvard-Smithsonian Center for Astrophysics, Cambridge, MA 01238, USA
Received 2009 April 9; accepted 2009 June 26; published 2009 July 24

ABSTRACT

We report on the properties of 89 low-mass star clusters located in the vicinity of luminous young clusters ("blue globulars") in the disk of M31. Eighty-two of the clusters are newly detected. We have determined their integrated magnitudes and colors, based on a series of *Hubble Space Telescope* (*HST*)/Wide Field Planetary Camera 2 exposures in blue and red (*HST* filters F450W and F814W). The integrated apparent magnitudes range from F450W = 17.5 to 22.5, and the colors indicate a wide range of ages. Stellar color–magnitude diagrams for all clusters were obtained and those with bright enough stars were fit to theoretical isochrones to provide age estimates. The ages range from 12 Myr to >500 Myr. Reddenings, which average E(F450 − F814) = 0.59 with a dispersion of 0.21 mag, were derived from the main-sequence fitting for those clusters. Comparison of these ages and integrated colors with single population theoretical models with solar abundances suggests a color offset of 0.085 mag at the ages tested. Estimated ages for the remaining clusters are based on their measured colors. The age–frequency diagram shows a steep decline of number with age, with a large decrease in number per age interval between the youngest and the oldest clusters detected.

Key words: galaxies: individual (NGC 224, M31, Andromeda) – galaxies: star clusters – galaxies: stellar content – Local Group

1. INTRODUCTION

This paper reports on the study of open (disk) star clusters in M31 (NGC224) detected on images from the *Hubble Space Telescope* (*HST*), obtained as part of a program designed to determine the nature of 19 luminous star clusters that were originally classified as globular clusters, but which have blue measured colors. The first paper of a series that reports on the results of that program concerns the highly luminous young cluster vdB0 (Perina et al. 2009). This paper is a survey of less luminous ("open") clusters in M31, similar to those of Krienke & Hodge (2007, hereafter KHI), who reported results from archival images obtained with the Wide Field Planetary Camera 2 (WFPC2), and Krienke & Hodge (2008, hereafter KHII), who reported results from archival images from the Advanced Camera for Surveys (ACS).

"Open" or "disk clusters" in M31 have been recognized since Hubble's pioneering work. He identified the cluster subsequently known as vdB0 as an open cluster, as shown in the frontispiece of his book "The Realm of the Nebulae" (Hubble 1936). Most subsequent studies of such clusters have dealt with the more luminous examples, especially those mistaken for globulars; see an excellent history of the subject of M31's luminous blue clusters in Caldwell et al. (2009).

As in Paper I, we adopt a distance modulus for M31 of $(m - M)_0 = 24.47 \pm 0.07$.

2. OBSERVATIONS

2.1. The Images

The observations, obtained with WFPC2 of the *HST,* were described in detail in Perina et al. (2009). The images were obtained with blue (*HST* F450W) and red (*HST* F814W) filters, approximately in the traditional B and I bands. Exposures were relatively short (2 × 400 seconds per filter). The scale of the WF fields is 0.099 arcsec pixel^{-1} and for the PC fields it is 0.045 arcsec pixel^{-1}. While the main program dealt with the bright globular-like clusters on the PC images, we searched both the PC and the WF images, identifying star clusters, measuring their integrated properties, and carrying out stellar photometry of their member stars. Figure 1, in a color version produced by one of us (T.P.), reproduces a sample WF field showing several open clusters. The total area covered by the survey is 48.1 arcmin^2.

2.2. Cluster Identification

The clusters included in the survey range from large, very luminous clusters to small objects that are barely resolved in our rather short exposures. The brightest disk clusters in this sample have absolute magnitudes of $M(\mathrm{F450})_0 = -8$, while we were able to identify a few clusters as faint as $M(\mathrm{F450})_0 = -2.5$. Thus our brightest clusters are equivalent to the mean absolute magnitudes of M31's globular clusters (though bluer and less massive), while our faintest are fainter than the faint limit of most cluster catalogs for nearby galaxies.

The disk of M31 presents a dense star field, in which low-density star clusters are difficult to detect even with special statistical techniques. For that reason we chose to select only conspicuous objects for which there would be little or no question of their being physical clusters (see examples in Figure 2). Our cluster identification criteria included (1) a conspicuous spatial concentration, (2) a centrally peaked radial distribution, (3) detectability in both colors, (4) recognition of more than four well-resolved stars above an unresolved background, (5) a normal luminosity distribution (number increasing with

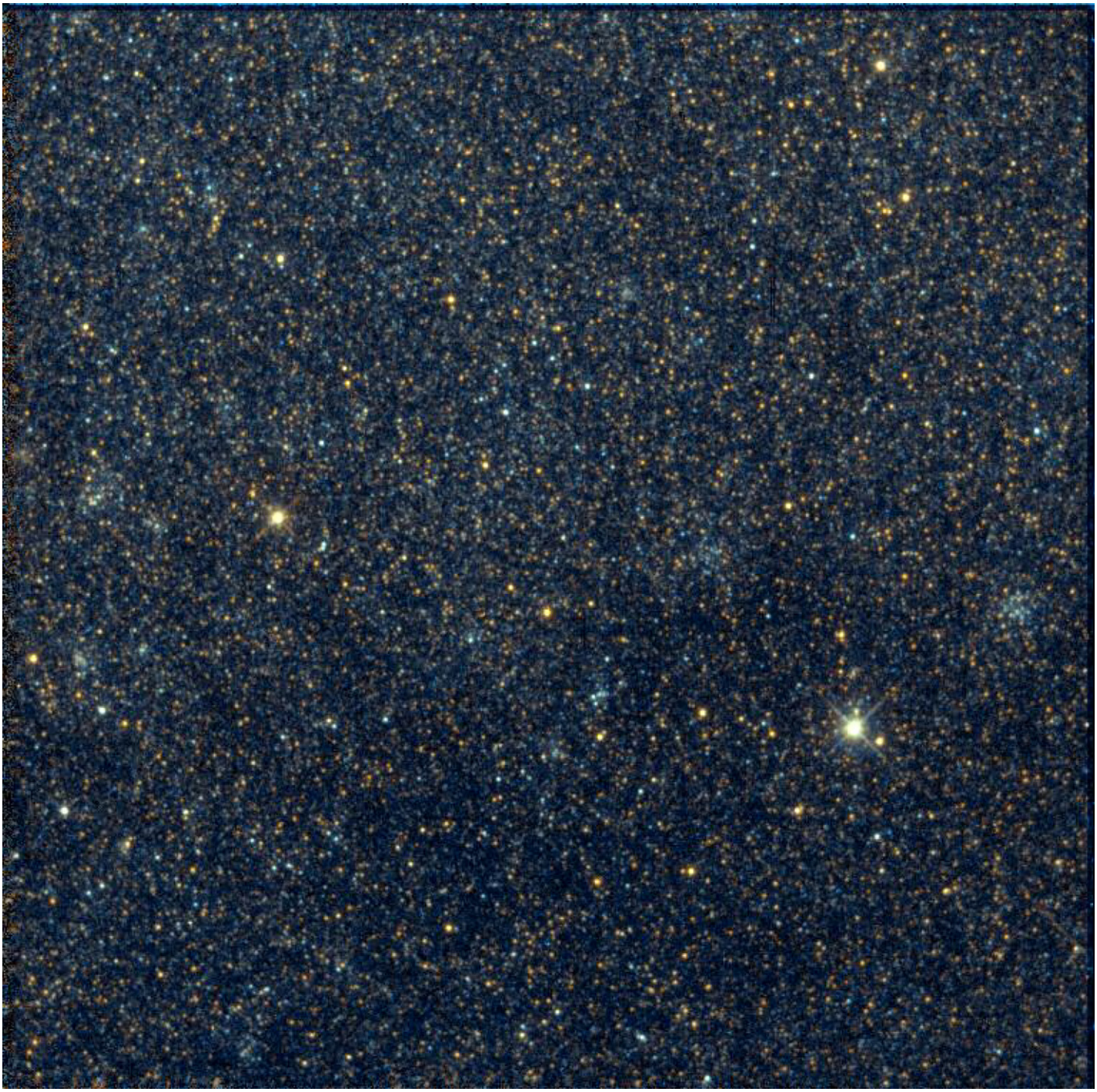

Figure 1. A sample WF image, containing several recognizable star clusters. This figure demonstrates how clusters are distinguished by their resolution, high stellar density, and blue color, compared to the background of the M31 disk stars.

magnitude), and (6) a color–magnitude diagram that shows a distribution different from that of the background.

Two of the authors (P.H. and O.K.K.) searched the frames independently in both colors, varying brightness and contrast. We categorized objects as definitely clusters or as candidates, and for borderline cases, we met, discussed images, and reached agreement.

As a final test, we asked each other whether we could defend an object against being classed as an asterism, background galaxy, or other type of noncluster. Figure 2 provides F450 images of 12 of the clusters.

3. DATA REDUCTION

3.1. Integrated Photometry

We determined integrated magnitudes and colors of the clusters using a photometric program written by Krienke in IDL and described in detail in KHI. Magnitudes in the *HST* photometric system were calibrated according to the results of Holtzman et al. (1995). The program determines the cluster properties within a contour chosen to include most of the light, but omitting any bright foreground stars. The critical feature of the photometry is determining the background surface brightness (the "sky").

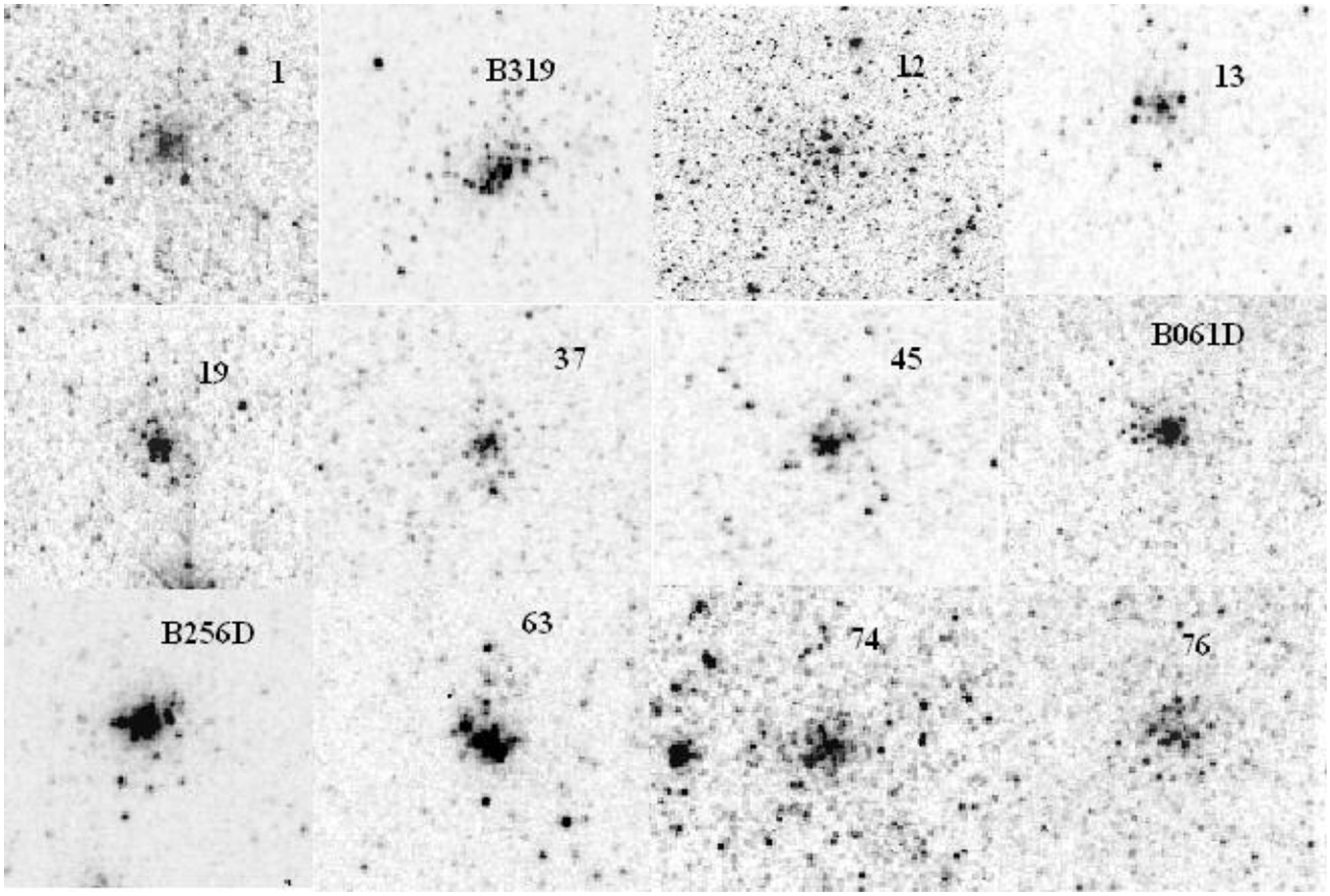

Figure 2. Images of 12 of the brightest clusters in the sample. Each small field is 7 arcsec on a side, except for cluster 12, for which the sides are 14 arcsec. The images are from the F450W filter and the WF camera.

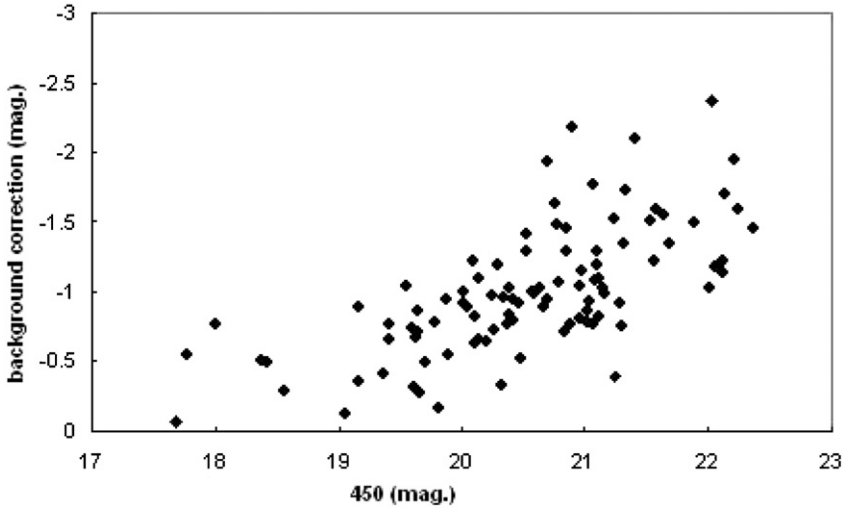

Figure 3. Background corrections plotted against the corrected integrated F450 magnitudes of the clusters. Magnitudes are not reddening-adjusted.

Because many of the clusters have both a low surface brightness and a significant size, the M31 background is often a significant fraction of the measured signal. Our program measures a probable background level and determines the uncertainty of it by sampling several (10–24) similarly dimensioned fields on the image. These data are refined by Chauvenet criteria, rejecting samples with less than 0.02 probability of belonging to the set. The average of the remaining values of the background is then flux subtracted from the total flux within the cluster contour. The correction to the magnitudes due to the background subtraction was usually several tenths of a magnitude, but in some cases, where the cluster surface brightness was especially faint compared to the background, it reached values as large as 2 mag (see Figure 3). Clearly, the background correction is an important element in this photometry and it is essential that it and its uncertainty be evaluated carefully. The photometric uncertainties provided in Figure 4 and Table 1 include that of the background, which, in some cases, dominates the uncertainty.

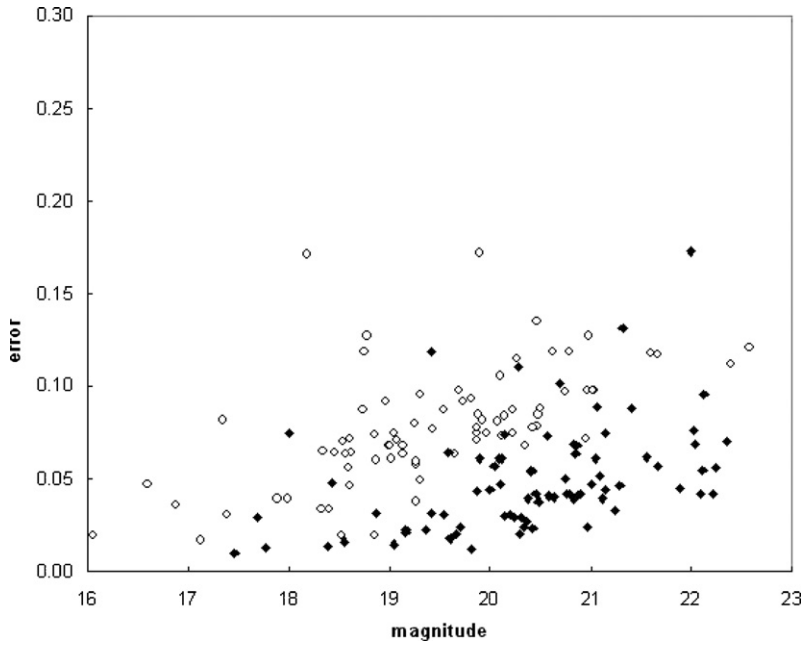

Figure 4. Photometric errors derived from the measurements of the integrated magnitudes, uncorrected for reddening. Filled symbols are for the F450 data and open symbols are for the F814 data.

3.2. Stellar Photometry

We carried out two independent programs of stellar photometry of the clusters. In one case, all of the WFPC2 images of each field were measured at Bologna as part of the luminous young clusters program. The details of that photometry are given in Paper I (Perina et al. 2009). For this paper we have extracted from the Bologna database the magnitudes and colors of stars within our outline of a cluster's boundary. Following the practice of Perina et al. (2009), we provide *HST* Vega magnitudes as measured in the two filters, which we refer to in the following as "F450" and "F814."

A second photometric program was carried out in Seattle using a program developed by one of us (O.K.K.), based on DAOPHOT (Stetson 1987) and written within IDL. It was adjusted to allow us to measure stars in the more crowded central areas of clusters, where there are often bright stars, frequently including the brightest main-sequence stars in the cluster. Without at least approximate photometry of these stars, we would be missing important information about the ages of the clusters. Zero points were adopted from Holtzman et al. (1995). PSFs were derived from several bright, well-separated stars in the field.

A comparison of the magnitudes and colors of the two sets of photometry showed good agreement. We identified stars in common by using both magnitudes and positions, finding that most bright stars were easily identified, while for the faintest stars there was sometimes an ambiguity. For stars with F450 magnitudes brighter than 23.0 the mean differences (Bologna-Seattle) were -0.12 ± 0.05 mag in F450 and -0.13 ± 0.11 mag in F814. At fainter magnitudes, where the photometry is strongly affected by crowding and by the short exposures of the images, the dispersion is larger. We have adjusted the Seattle photometry to the Bologna system by using the above offsets.

4. PROPERTIES OF THE CLUSTERS

4.1. The Cluster Catalog

Table 1 provides the positions, integrated magnitudes, and integrated colors of the clusters. Five of the clusters were found to have been identified previously according to the Revised Bologna Catalog of M31 Globular Clusters (Galleti et al. 2004, hereafter RBC). One of them, DAO84, was identified as a possible galaxy by Caldwell et al. (2009), but our images show a clearly defined star cluster. Additionally, one coincides with an open cluster identified in KHI and one to a cluster discovered by Williams & Hodge (2001b). Only two of the previously identified clusters, B319 and KH22, had published magnitudes in B and only B319 had previously published magnitudes in both B and I. We transformed our magnitudes to Johnson–Cousins B and I for comparison. The average difference (previous – this paper) in B was found to be 0.16 mag. and the difference in I is 0.18 mag.

As a ground-based check on the *HST* photometry, one of us (J.S.) determined the integrated magnitudes and colors of 16 of the brighter clusters from the SDSS database. Measures were obtained in the SDSS system (u, g, r, i, z) and transformed to B and I in the J–C system. All measures used a circular aperture with a radius of 4 arcsec. The measures produced data that agreed fairly well with mean differences (CfA-Seattle) of $\Delta B = -0.24 \pm 0.39$ and $\Delta(B - I) = 0.23 \pm 0.14$. Experiments with *HST* photometry using a 4 arcsec aperture indicated that the differences are probably caused at least partly by nearby bright stars that were avoided by the original *HST* photometry, which used smaller apertures.

4.2. The Integrated Cluster Color–Magnitude Diagram

Figure 5 shows the color–magnitude diagram (hereafter CMD) of the present sample (we include in this diagram and in Figure 6 two clusters from the main target program, which were found serendipitously on the WF frames). It closely resembles the two diagrams published for similar samples of M31 clusters by KHI and KHII, though with different filter pairs. The mean absolute magnitude for the cluster sample plotted is $M(\mathrm{F450})_0 = -4.59$ and the mean unreddened color is $(\mathrm{F450} - \mathrm{F814})_0 = 0.67$.

The clusters are nearly uniformly distributed over the diagram, but with a mild concentration at about F450 = 21 and F450 – F814 = 1. For reference, a cluster with observed values of F450 = 21.0 and F450 – F814 = 1.0 will have an age of about

Table 1
Star Clusters of the Survey

Name	R.A. (J2000)	Decl. (J2000)	F450	Err	F450 – F814	Err	Notes
KHM31–22	9.99416	40.59044	20.36	0.03	1.38	0.07	
1	10.00226	40.59630	20.00	0.04	1.48	0.05	
B319	10.01277	40.56638	17.77	0.01	0.89	0.04	
WH	10.03147	40.58568	20.75	0.05	0.64	0.09	
2	10.05996	40.47970	21.10	0.05	0.11	0.12	∗y
3	10.06724	40.46574	20.87	0.07	0.72	0.11	y
4	10.07673	40.46278	20.23	0.03	0.93	0.06	y
5	10.08475	40.47733	21.29	0.05	0.81	0.10	y
6	10.09359	40.46366	22.10	0.04	0.50	0.13	y
7	10.10565	40.61191	21.23	0.13	−1.01	0.18	∗y
8	10.12093	40.60816	20.31	0.03	0.67	0.07	y
9	10.12172	40.62505	20.68	0.08	0.30	0.13	∗y
10	10.12880	40.62470	20.26	0.04	0.01	0.11	∗y
11	10.13828	40.61543	21.08	0.10	1.06	0.15	
12	10.14448	40.61308	18.00	0.08	1.42	0.09	y
13	10.15506	40.65390	19.36	0.02	1.47	0.05	y
14	10.15727	40.66958	20.83	0.04	1.71	0.06	y
15	10.17087	40.65345	20.96	0.06	0.74	0.11	∗
B014D	10.25410	41.10937	19.60	0.02	1.63	0.04	
16	10.25739	41.12103	21.01	0.05	1.14	0.09	y
17	10.26360	41.11692	21.11	0.04	1.15	0.08	
18	10.27091	41.11649	20.42	0.02	1.16	0.04	y
19	10.27805	41.12904	19.41	0.12	1.23	0.21	y
20	10.31100	41.11747	22.03	0.08	1.23	0.14	y
21	10.32247	41.11345	20.69	0.10	1.95	0.16	y
22	10.32486	41.10686	21.40	0.09	1.18	0.12	y
23	10.32638	41.09547	21.88	0.05	1.60	0.10	
24	10.40369	40.72710	21.31	0.04	−0.36	0.12	∗y
25	10.40514	40.68031	20.56	0.07	1.42	0.10	y
26	10.41120	40.73322	18.55	0.02	0.21	0.07	∗y
27	10.41445	40.67577	19.81	0.01	1.11	0.03	y
28	10.41904	40.72756	21.63	0.03	−0.95	0.12	∗y
29	10.42279	40.66916	20.19	0.03	0.92	0.07	y
30	10.42782	40.71453	19.66	0.02	0.69	0.07	y
31	10.43303	40.71460	21.08	0.04	0.12	0.11	∗
32	10.43314	40.71762	21.09	0.05	1.22	0.09	y
33	10.43358	40.71122	20.89	0.04	2.04	0.09	
34	10.43870	40.72325	20.38	0.04	1.33	0.08	y
35	10.44996	40.71653	20.79	0.04	0.70	0.11	y
36	10.45031	40.69453	21.05	0.06	0.59	0.10	y
37	10.45168	40.69946	19.16	0.02	0.38	0.07	y
38	10.45521	40.72142	20.66	0.04	0.27	0.10	∗y
39	10.45635	40.73367	21.08	0.26			y
40	10.46038	40.70244	20.58	0.04	0.69	0.09	y
41	10.51435	40.76969	20.14	0.03	1.53	0.08	
42	10.51689	40.74818	21.25	0.03	0.82	0.09	y
43	10.52399	40.77104	21.15	0.04	1.22	0.09	y
44	10.52901	40.76606	20.84	0.07	1.58	0.09	y
45	10.52987	40.76940	19.17	0.02	0.71	0.07	y
46	10.53052	40.77541	20.95	0.04	0.37	0.10	∗y
47	10.53562	40.77516	19.70	0.02	0.71	0.07	y
48	10.55479	40.82819	20.63	0.04	1.20	0.09	
49	10.57024	40.81240	20.76	0.04	1.22	0.10	y
50	10.57764	40.81500	22.11	0.06	1.08	0.11	
51	10.57851	40.81922	19.89	0.06	1.35	0.09	
B061D	10.63578	41.36173	19.41	0.03	0.67	0.09	∗
52	11.10224	41.25305	20.34	0.02	1.73	0.05	
53	11.11621	41.23792	20.96	0.02	2.11	0.03	
54	11.12238	41.23356	22.21	0.04	1.86	0.08	
55	11.22630	41.88489	21.28	0.04	0.19	0.10	∗
56	11.23180	41.91120	20.29	0.02	0.92	0.04	
57	11.23438	41.89684	22.04	0.07	2.31	0.12	
58	11.23474	41.89572	20.11	0.06	1.15	0.11	y
59	11.23536	41.88171	20.45	0.04	2.06	0.05	
60	11.23619	41.91635	20.41	0.05	1.80	0.08	
61	11.24062	41.89716	22.12	0.10	1.38	0.14	y

Table 1
(Continued)

Name	R.A. (J2000)	Decl. (J2000)	F450	Err	F450 – F814	Err	Notes
B256D	11.24448	41.91018	17.57	0.02	1.58	0.03	
62	11.24560	41.89819	20.09	0.06	0.84	0.10	y
63	11.24637	41.91047	19.05	0.02	1.93	0.02	
64	11.24650	41.91050	18.87	0.03	1.88	0.05	
65	11.24744	41.89167	21.55	0.07	−0.84	0.13	∗y
66	11.24854	41.90391	20.21	0.09	1.43	0.12	y
67	11.24969	41.93580	20.85	0.06	0.78	0.10	y
68	11.24973	41.90117	21.32	0.13	1.06	0.17	y
69	11.25109	41.90682	21.06	0.09	1.17	0.19	y
70	11.25216	41.88646	20.48	0.04	1.17	0.10	y
71	11.25366	41.88541	19.87	0.04	0.85	0.08	y
72	11.25606	41.89460	21.76	0.13	0.76	0.17	
73	11.25914	41.91537	19.97	0.04	1.31	0.07	
74	11.26204	41.89759	20.52	0.09	0.67	0.12	y∗
75	11.26219	41.90101	20.38	0.08	−0.08	0.16	∗y
76	11.26942	41.89441	20.02	0.06	1.03	0.11	
77	11.28053	41.90742	21.67	0.06	0.83	0.11	y
78	11.28957	41.91235	21.56	0.06	0.61	0.10	y
79	11.29089	41.91942	20.10	0.05	1.50	0.07	y
80	11.43302	41.72510	19.63	0.03	0.55	0.08	y
81	11.45692	41.71174	22.35	0.07	1.85	0.11	
82	11.45853	41.70832	22.23	0.06	1.61	0.13	
DA084	11.46799	41.71365	19.59	0.06	0.81	0.14	

Notes. Objects with asterisks have uncertain colors because of a low ratio of signal to galaxy background in the F814W image. Objects with "y" have CMDs indicating young ages, less than $\sim 5 \times 10^8$ years.

∼70 Myr and a mass of 450 solar masses, assuming a Salpeter stellar luminosity function and Girardi (2006) population models. But note that the age–color diagram is multivalued at these colors (see Section 5.2).

The mean size of the isophotal radii of all clusters was 1.61 arcsec (6.12 pc).

4.3. The Integrated Cluster Luminosity Function

The luminosity function of the clusters is shown in Figure 6, where the magnitudes are corrected for extinction, assuming a mean reddening of F450 – F814 of 0.51 (see Section 6). The shape of the luminosity function is approximately Gaussian, with a maximum at $M(\mathrm{F450})(0) = -4.2$. All three samples show an enhanced frequency at the bright end, compared to a symmetrical curve. Artificial cluster tests on the WFPC2 *HST* images in KHI indicated that much of the turn-down at faint magnitudes results from detection limits. It is not yet clear what the shape of the true luminosity function is at such faint limits. While KHI suggested that the luminosity function may continue to rise, at least to $M(\mathrm{F450}) = -1$, similar *HST* searches for faint clusters in the SMC have produced contrary results (Rafelski & Zaritsky 2005). In any case, the luminosity function at the faint end is a complicated product of selection effects, evolutionary fading rates and dynamical disruption (Hunter et al. 2003).

4.4. Individual Cluster CMDs

As described in Section 3.2, we measured stellar CMDs for all clusters. Most diagrams looked reasonable, but not all of the clusters were well enough resolved to allow meaningful interpretation. Especially for the faintest clusters, the number of stars on the F814 frame was often quite small, on the order of 5–10.

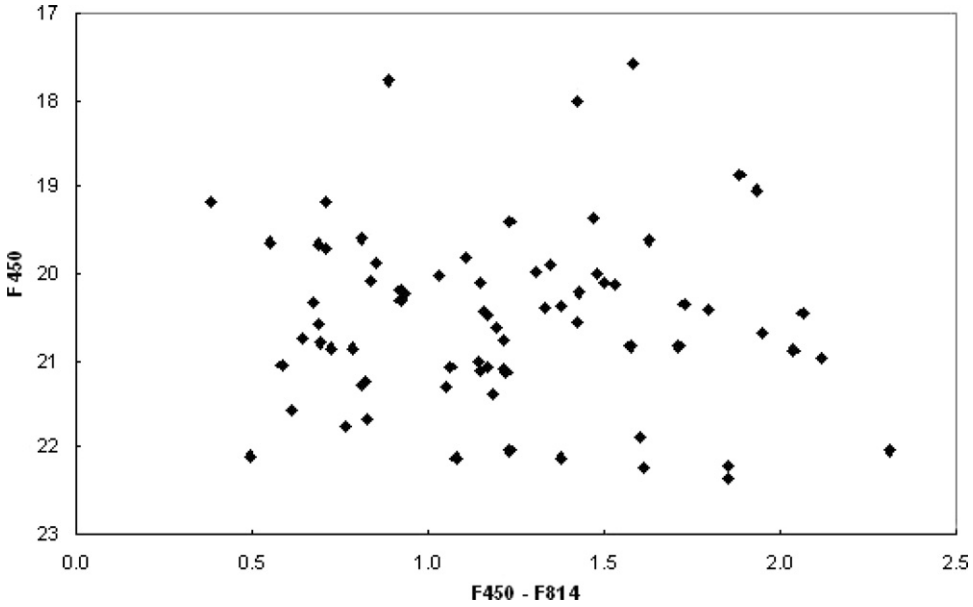

Figure 5. CMD for the integrated colors and magnitudes of clusters in this survey. The plot shows observed values, before corrections for reddening.

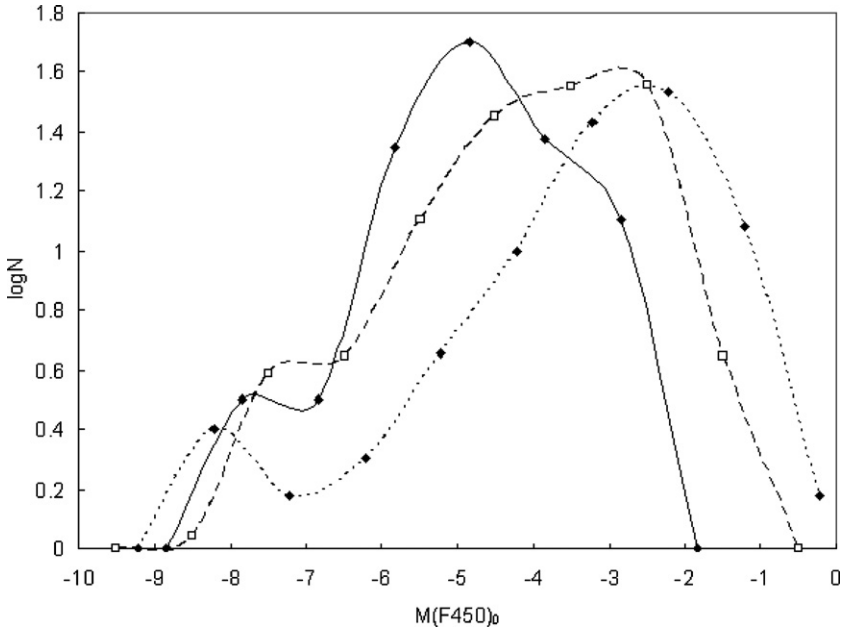

Figure 6. Luminosity function for the clusters of this survey (solid line) compared to that of KHI (dotted line) and KHII (dashed line). The latter two are normalized to the total number of clusters in the present survey.

Figure 7 shows the CMDs for 10 clusters for which the CMDs show a well defined main sequence. These clusters show a main sequence with F450 – F814 near 0.5 and with the tip of the main sequence in the range with F450 magnitudes = 20 to 24. The CMDs in Figure 7 have been adjusted for reddening (see Section 5.1).

Table 2 lists the clusters for which it was possible to determine age and reddening by comparison with the Girardi models. The quoted uncertainties indicate the extreme limits of acceptable fits judged by eye.

One of the clusters, B319 (also known as G44) has been studied previously using other *HST* images (Williams & Hodge 2001a). The present CMD is shallower and it covers only the central region of B319, but the two CMDs are morphologically similar. We cannot usefully make detailed comparisons because the Williams & Hodge data were taken with different filters (F 336W, F439W, and F555W).

A careful inspection of the CMDs of the clusters and their surrounding fields shows that the degree of contamination of the cluster MS by field stars is negligibly low and does not affect our estimates of age and reddening.

5. AGES AND REDDENINGS

5.1. From the CMDs

For clusters with a sufficiently well-defined sequences of stars, especially young clusters with narrow main sequences, it was possible to determine approximate reddenings and ages. Based on the case for vdB0 (Perina et al. 2009), we assumed that

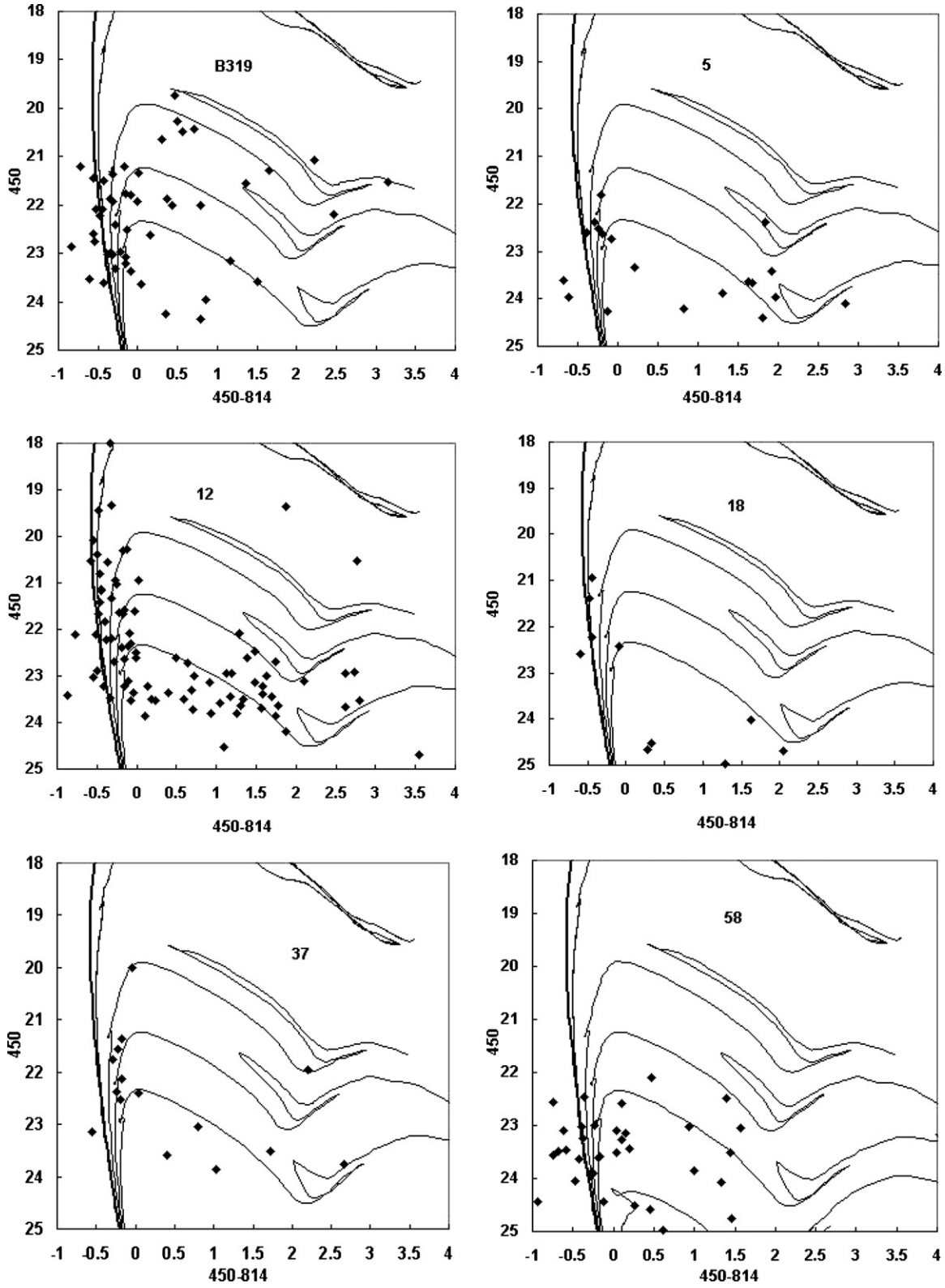

Figure 7. CMDs for 10 young clusters with well defined main sequences, fitted by eye to Girardi (2006) isochrones for solar abundance and ages with log(age) of 7.0, 7.6, 8.0, 8.25, and 8.7 years.

these young clusters are characterized by solar abundances. We compared the observations with evolutionary model isochrones made available from the Padua Web page (Girardi 2006) and determined the offset by eye, providing approximate values of age and reddening (Table 3). Because of the faintness of the magnitudes, the crowding and the sparseness of the CMDs, these values have fairly large uncertainties, as quoted in the table. Within the accuracy of the fitting and if our assumption of solar abundances is correct, the fits provide individual reddenings for the selected clusters, which range from $E(\mathrm{F450} - \mathrm{F814}) =$

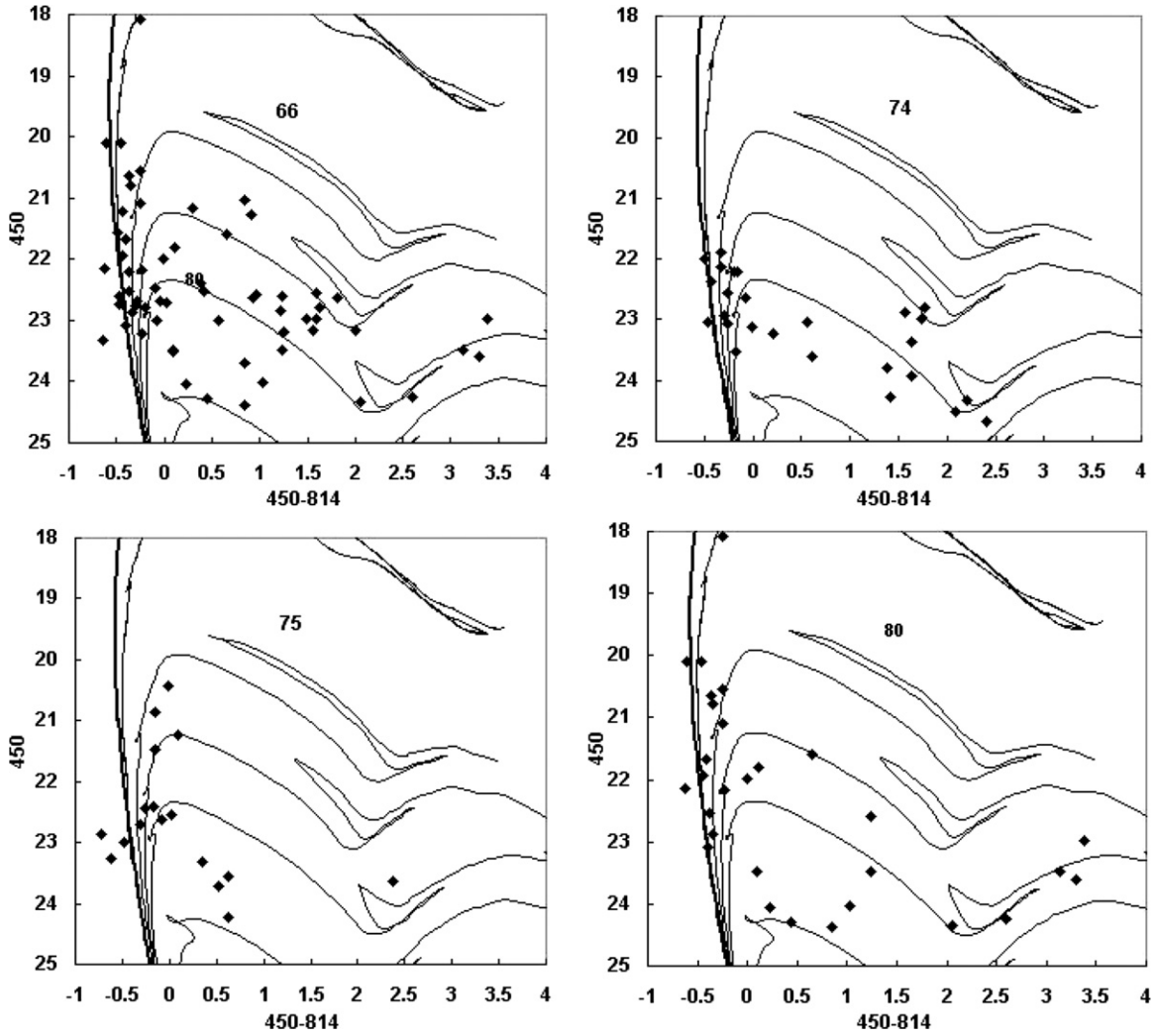

Figure 7. (Continued)

0.25 to 0.85, with a mean uncertainty of 0.23. The average reddening for this sample is 0.59 with a standard deviation of 0.21 mag. Selection effects, of course, severely limit our sample of clusters with bright main sequences to the youngest clusters in the sample; most are younger than 200 million years.

For the remaining clusters in the sample, the CMDs are difficult to interpret in terms of ages and reddenings except in approximate terms. Table 1 notes those clusters that have significant numbers of stars in the blue section of their CMDs to indicate that they are younger than a few times 10^8 years. Most of the remaining clusters are older, as is also indicated by their integrated colors.

5.2. From the Integrated Cluster Photometry

Integrated colors of open clusters can be used to estimate cluster ages by comparison with theoretical models. There are a number of problems with this procedure in our case:

1. The colors are intrinsically uncertain because of the spatially variable brightness and color of the M31 background, which is the major source of the photometric uncertainty.
2. The theoretical models show a dependence on the elemental abundances, which are unknown.
3. For young small-mass clusters, the colors depend on small number statistics in the presence or absence of the most luminous blue stars or a few red giants (see Frogel et al. 1983 and Cervino & Luridiana 2004 for quantitative treatments of this problem).
4. Different theoretical models, even for the same abundances, give different relationships for the age–color diagram.
5. For the colors used in this program (F450 and F814), the change with color for young clusters ($< 2 \times 10^8$ yr) is multivalued for some regimes and is generally smaller than the measurement uncertainties (Figure 8).

In spite of these difficulties, it is possible to estimate approximate ages from the colors and, for the younger clusters, the average reddening. Figure 8 shows the colors of the clusters with well defined main sequences compared to the theoretical colors for single-age populations with solar abundances (Girardi 2006). The colors plotted are the measured colors corrected for reddening and the reddening and ages are those determined from main-sequence fitting. The colors cluster close to the theoretical distribution but are clearly offset to the blue. This may be due to abundances that are different from our assumption of solar abundance ratios. Alternatively, if we assume the offset to be due to overestimation of reddening, then the best fit to the models is for a mean reddening 0.085 mag smaller than derived from the MS fitting, and gives a mean reddening of E(F450 – F814) = 0.50 (this corresponds to $E(B - V) = \sim 0.25$).

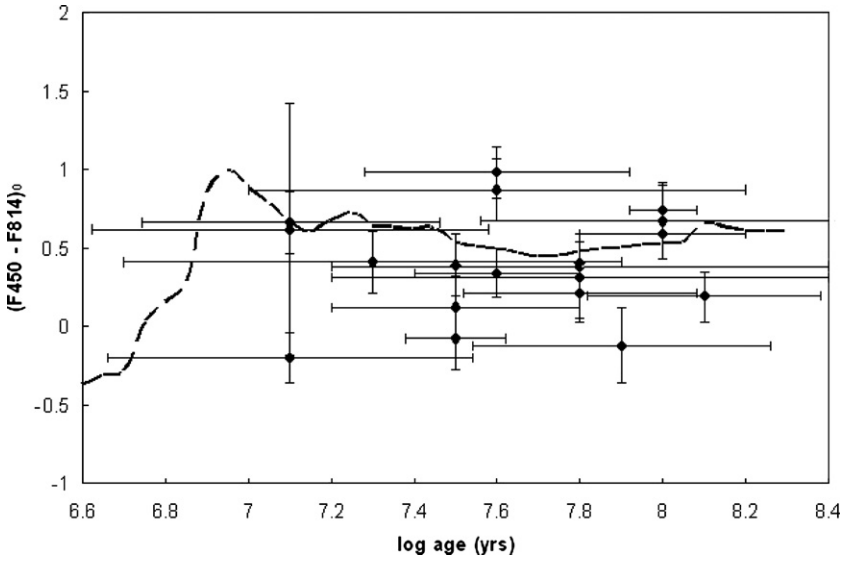

Figure 8. Ages and reddening-corrected colors determined from MS fitting compared to the theoretical age–color relationship for young clusters (Girardi 2006).

Table 2
Characteristics of Cluster CMDs with Well Defined Main Sequences

Cluster no.	log age (yrs)	Uncertainty	E(F450 – F814)	Uncertainty
KH22	7.6	0.35	0.4	0.15
B319	7.6	0.5	0.5	0.25
3	7.5	0.45	0.8	0.2
5	8.0	0.6	0.5	0.3
8	7.5	0.35	0.55	0.2
11	7.3	0.6	0.5	0.2
12	7.6	0.6	0.55	0.25
13	7.1	0.5	0.85	0.8
18	7.1	0.35	0.5	0.2
34	8	0.45	0.65	0.25
37	7.9	0.35	0.5	0.25
45	7.8	0.3	0.5	0.15
B061D	7.8	0.6	0.5	0.15
58	7.6	0.2	0.8	0.15
62	8.0	0.2	0.25	0.15
68	7.8	0.3	0.82	0.15
74	8.1	0.3	0.65	0.15
75	7.8	0.5	0.5	0.25
80	7.1	0.45	0.75	0.15

For our complete sample we adopt this value for the mean reddening.

For ages of clusters older than ∼300 million years the theoretical curve is single-valued and fairly sensitive to the measured colors. Because of our shallow exposures, it is not possible to derive ages from CMDs for these clusters, but we can estimate ages from colors, if we assume a mean reddening and a particular model set and abundance. Table 3 provides approximate ages for the clusters with colors redder than (F450 – F814) = 1.0. These data are calculated with a mean reddening of E(F450 – F814) = 0.50 and use the models provided by Girardi (2006). Formal errors of the colors correspond to approximately an uncertainty of 0.10 in log age, but the true uncertainties of the ages are considered to be much larger, for the reasons outlined at the beginning of this section. The reddest clusters in the sample have reddening-corrected colors of F450 – F814 = ∼1.8, which corresponds to an age of approximately 1.5×10^9 years.

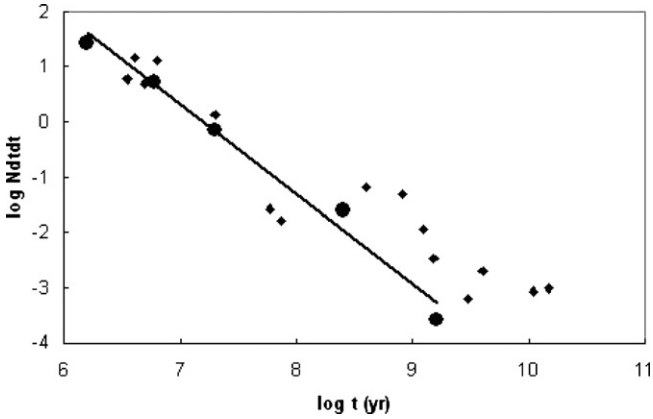

Figure 9. Age distribution for the clusters in this survey (large circles) compared to that reported in KHI (diamonds). The line is a least-squares linear fit to this paper's data.

5.3. The Age Distribution

We have suggested above that the CMD of integrated magnitudes (Figure 5) indicates that the clusters are not distributed uniformly in age. To examine the age distribution we have combined the age data for the young clusters based on main-sequence fitting with that for older clusters based on colors. Figure 9 shows the distribution for our sample of 82 clusters. The number falls off rapidly with age, approximately exponentially. A least-squares linear fit gives

$$\log(N) = -1.625 \log(t) + 11.676.$$

Also shown in Figure 9 is a similar curve for the clusters in KHI, where the number has been normalized to adjust for that survey's larger sampling area. The two agree within their errors, though there is a suggestion of a small difference in slope, which is possibly caused by the shallower exposure times of the present survey, which probably missed a larger fraction of older clusters.

As discussed briefly in KHI and in a large and diverse recent literature, these kinds of data are useful for determining the survival rate of clusters in a galaxy's gravitational field (e.g., Kruijssen & Lamers 2008; Gieles et al. 2006; Chandar et al. 2006; Lamers & Gieles 2006 and many others). Before such

Table 3
Ages for Older Clusters Based on Integrated Colors

Name	log age (yrs)
1	8.63
14	8.77
B014D	8.72
16	8.29
17	8.30
19	8.38
20	8.38
21	8.94
22	8.33
23	8.70
25	8.56
27	8.25
32	8.37
33	8.97
34	8.50
41	8.64
43	8.37
44	8.68
48	8.37
49	8.38
50	8.22
51	8.50
52	8.79
53	9.04
54	8.87
57	9.22
59	8.99
60	8.84
61	8.53
B256D	8.68
63	8.92
64	8.88
66	8.57
69	8.32
70	8.32
73	8.46
76	8.15
79	8.63
81	8.87
82	8.71

use can be made of the data, however, it is necessary to know both the rate of evolutionary fading of the clusters and the detection efficiency of the survey. We note that the fading rate is dependent on the abundances, which are unknown, and the detection efficiency is dependent on the exposure times, on the structural properties of the clusters and on the background surface brightness and its variability. To determine the detection efficiency for a collection of such faint and varied clusters would require a much larger sample, as each of the determining factors would need to be explored. In view of these difficulties, we believe that the current survey is not appropriate for deriving a tidal destruction rate for M31 clusters.

6. SUMMARY

This paper supplements the *HST*/WFPC2 Survey of Luminous Young Clusters in M31, which examines the nature of 19 globular-like objects that are anomalously blue. Our search for other, less luminous clusters on the images has produced a catalog of 89 clusters, 82 of which are newly identified.

We have obtained integrated magnitudes and colors of the clusters and have measured CMDs for their resolved stars. The absolute magnitudes of the clusters range from $M(\mathrm{F450}) = -8$ to -2.5 and their colors indicate a large range of ages, from a few million to a few times 10^9 years. The richest young clusters have well-defined main sequences that have been fitted to theoretical isochrones, providing ages ranging from approximately 12 million to 100 million years. The CMDs of these clusters indicate reddenings averaging $E(\mathrm{F450} - \mathrm{F814}) = 0.59$, with a dispersion of 0.21 mag, while a comparison of integrated colors of a larger sample of the young clusters with theoretical population models indicates a somewhat smaller average reddening of 0.50 mag. We derive a cluster luminosity function that shows a peak value of $M(\mathrm{F450})_0$ of -4.2 and which extends from values of -9 to -2. The least luminous clusters are among the faintest measured for clusters in LG galaxies. There is a suggestion of a small number of anomalously luminous clusters at the bright end of the luminosity function. The distribution of the number of detected clusters with age shows a very steep gradient.

This paper was based on observations made with the NASA/ESA *Hubble Space Telescope*, obtained at the Space Telescope Institute, which is operated by the Association of Universities for Research in Astronomy, Inc. under NASA contract NAS 5-26555. These observations are associated with program GOI-10818 (PI: J. G. Cohen) and were partially funded under that program.

REFERENCES

Caldwell, N., Harding, P., Morrison, H., Rose, J., Schiavon, R., & Kriessler, J. 2009, AJ, 137, 94
Cervino, M., & Luridiana, V. 2004, A&A, 413, 145
Chandar, R., Fall, M., & Whitmore, B. 2006, ApJ, 650, L111
Frogel, J. A., Cohen, J. G., & Persson, S. E. 1983, ApJ , 275, 773
Galleti, S., Federici, L., Bellazzini, M., Fusi Pecci, F., & Macrina, S. 2004, A&A, 416, 917
Gieles, M., et al. 2006, MNRAS, 371, 793
Girardi, L. 2006, http://pleiadi.pd.astro.it
Holtzman, J., Burrows, C., Casertano, S., Hester, J., Trauger, J., Watson, A., & Worthey, G. 1995, PASP, 107, 1065
Hubble, E. 1936, Realm of the Nebulae (New Haven, CT: Yale Univ. Press), frontespiece
Hunter, D. A., Elmegreen, B. G., Dupuy, T., & Mortonson, M. 2003, AJ, 126, 1836
Krienke, O. K., & Hodge, P. W. 2007, PASP, 119, 7 (KHI)
Krienke, O. K., & Hodge, P. W. 2008, PASP, 120, 1 (KHII)
Kruijssen, J., & Lamers, H. 2008, in ASP Conf. Ser. 396, Formation and Evolution of Galaxy Disks, ed. J. G. Funes & E. M. Corsini (San Francisco, CA: ASP), 149
Lamers, H. J. G. L. M., & Gieles, M. 2006, A&A, 455, L17
Perina, S., et al. 2009, A&A, 494, 933
Rafelski, M., & Zaritsky, D. 2005, AJ, 129, 2701
Stetson, P. 1987, PASP, 99, 191
Williams, B. F., & Hodge, P. W. 2001a, ApJ, 548, 190
Williams, B. F., & Hodge, P. W. 2001b, ApJ, 559, 851